A EUROPEAN JOURNAL

CHEMPHYSCHEM

OF CHEMICAL PHYSICS AND PHYSICAL CHEMISTRY

# Accepted Article

**Title:** Substituent Directed ESIPT Coupled AIE in NIR Emitting Quinazoline Derivatives

**Authors:** Bhupendra Kumar Dwivedi, Vishwa Deepak Singh, Rajendra Prasad Paitandi, and Daya Shankar Pandey



**To be cited as:** *ChemPhysChem* 10.1002/cphc.201800579

**Link to VoR:** http://dx.doi.org/10.1002/cphc.201800579

A Journal of ChemPubSoc Europe

WILEY-VCH www.chemphyschem.org

# Substituent Directed ESIPT Coupled AIE in NIR Emitting Quinazoline Derivatives

Mr. Bhupendra Kumar Dwivedi, Mr. Vishwa Deepak Singh, Dr. Rajendra Prasad Paitandi, and Prof. Dr. Daya Shankar Pandey*

Department of Chemistry, Institute of Science, Banaras Hindu University, Varanasi –221 005, (U. P.) India

**Abstract**

A series of ESIPT active systems (**HQz1**–**HQz6**) derived from quinazoline have been reported. The ESIPT emission for these derivatives gets completely quenched in solvents with diverse polarities which have been restored *via* AIE with large Stokes shift (up to 314 nm). It varied from 450 to 701 nm just by altering substituents at the para position of hydroxy group in the central phenyl ring. As well, **HQz1**–**HQz6** displayed solid-state emission [~ 455 (blue) to ~704 nm (red)]. The formyl group on the central hydroxy-phenyl ring of these derivatives induces ESIPT by increasing acidity of the hydroxy proton which has been followed by $^{1}$HNMR studies. Further, it has been clearly shown that emission colour and aggregate morphology can be fine tuned by incorporating apt substituents. The present study offers a simple route to obtain colour tunable ESIPT emission *via* AIE which is very important for biological imaging and fabrication of optoelectronic devices.

*Corresponding author: E-mail: dspbhu@bhu.ac.in

## Introduction

Red/NIR emitting organic scaffolds in solution/aggregated state with large Stokes shift have attracted immense current attention due to their potential applications in diverse areas.[1] The phenomenon of excited state intramolecular proton transfer (ESIPT) firstly reported by Waller et.al, has emerged as an attractive tool for creating the system with desired photophysical properties.[2] It represents typical photo-tautomerization arising from strong intramolecular H-bonding interactions leading to an excited keto tautomer with unique emission and large Stokes shift. The ESIPT systems have fascinated many groups due to their broad and dual emission, colour tunability, ultrafast process, extremely large Stokes shift and usefulness in developing new probes.[2] Despite fulfilling the structural requirements for ESIPT process, application of many organic systems has been marred due to the complete frustration of ESIPT emission.[3] Partial quenching of the ESIPT emission may occur in protic solvents due to stabilization of enol form *via* intermolecular H-bonding with solvent molecules. But, the complete frustration of ESIPT emission in polar as well as non-polar solvents is very annoying to the researchers.[3] Usually, the complete frustration of ESIPT emission can occur in extended π-conjugated systems.[3] Therefore its restoration is a must as it may improve their applicability in diverse areas. Further, it is presumed that aggregation-induced emission (AIE) which has been promising towards developing solid-state luminescent materials, particularly optoelectronic devices, may facilitate recovery of frustrated ESIPT emission.[4] On the other hand, aggregation-caused quenching (ACQ) opposite to AIE is a detrimental phenomenon which causes fluorescence quenching in aggregated state and hampers practical applications of fluorophores.[5] Thus, designing and development of ESIPT active systems offering creditable photophysical properties in solid/aggregated states are highly desirable. In this context, various research groups have developed systems displaying AIE and examined their applications.[4] Besides fluorescence revival in red/NIR region, AIE for ESIPT systems has scarcely been investigated.[2a]

Moreover, it has been realized that designing ESIPT coupled AIE system may offer a convenient route for the restoration of ESIPT emission and achieve red/NIR emissive organic materials with extremely large Stokes shift. The ESIPT fluorophores displaying long-wavelength emission (550–900 nm) in red/NIR region and large Stokes shift are advantageous in biology.[6] Further, quinazoline skeleton represents an important class of biologically active compounds commonly found in naturally occurring alkaloids.[7] These find wide applicability as hypnotic, analgesic, sedative, anti-diabetic, anti-bacterial, anti-

inflammatory, anticancer, antitumor, antiviral and anti-tubercular agents.[8] Moreover, reports dealing with quinazoline derivatives exhibiting ESIPT are rather scarce.

Through this work, an attempt has been made to develop novel NIR emitting quinazoline derivatives exhibiting ESIPT coupled with AIE. The ESIPT emission in these derivatives is completely frustrated in polar as well as non-polar solvents and restored through AIE. In this direction, systems have been modified in such a way that central hydroxy-phenyl group can act as a proton donor for the quinazoline and/or formyl group in the ESIPT process.[9] As shown in scheme 1, **HQz1–HQz6** can undergo switching of an intramolecular proton transfer between the central hydroxy-phenyl proton and either the quinazoline or the formyl group upon changing the substituent (R1) on the central hydroxy-phenyl ring and thereby opens a new possibility of fluorochromism.[9c] An amalgamation of electron donating and electron withdrawing group *p*-to the hydroxy group of central phenyl ring causes a red and blue shift for AIE maxima respectively. Through this contribution, we describe synthesis, characterization and photophysical properties of a series of novel quinazoline-based organic scaffolds exhibiting ESIPT coupled AIE with large Stokes shift (~ 314 nm).[8] Such NIR systems may find potential applications, in biology especially in the *in-vivo* studies and optoelectronics.[10]

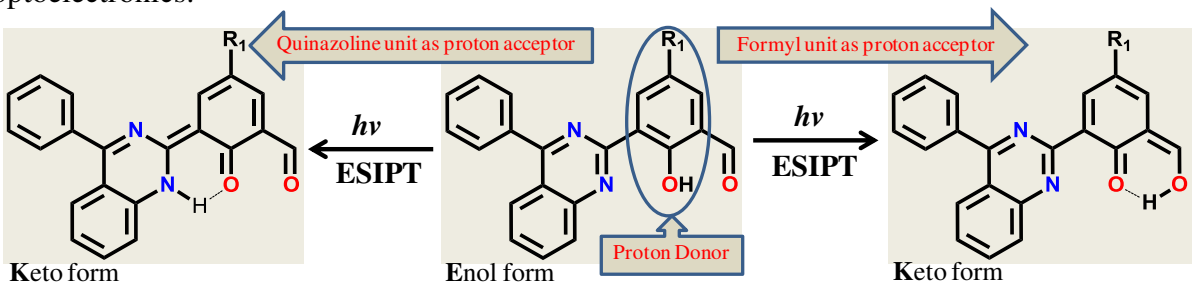


**Scheme 1**. Intramolecular proton transfer switching between two ESIPT sites (quinazoline and formyl unit) and resulting keto species.

## Results and Discussion

### Synthesis and Characterisations

The quinazoline derivatives (**3a**–**3e**) have been synthesized by reaction of 2-aminoaceto-phenone (1) and corresponding 5-substituted salicylaldehydes (**2a**–**2e**) following reported procedures.[11] These reacted with hexamethylenetetramine in trifluoroacetic acid to afford derivatives of 2-hydroxy-3-(quinazolin-2-yl)-benzaldehyde (**HQz1**–**HQz6**) in moderate to very good yield (39% to 96%).[12] Methoxy derivative (**Qz-OMe**) has been obtained by treatment of **HQz3** with iodomethane in presence of $K_2CO_3$ in dry DMF.[13] The simple

strategy adopted for the synthesis of the compounds is shown in Scheme 2. The compounds under investigation exhibited good solubility in THF, acetonitrile, DMF, DMSO, and dichloromethane, are moderately soluble in methanol, ethyl acetate and are poorly soluble in non-polar solvents. These compounds have been thoroughly characterized by IR, HRMS, and $^{1}H/^{13}C$ NMR spectroscopic studies (Figures S1–S19).

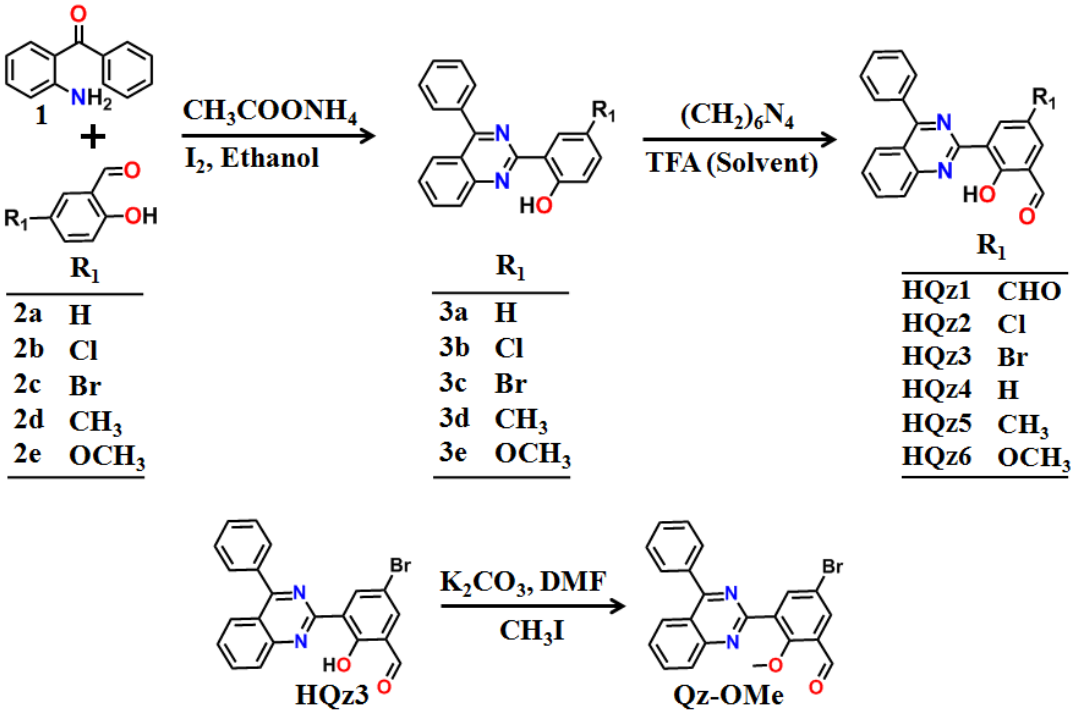


**Scheme 2**. A schematic representation of the synthetic route adopted for quinazoline derivatives (**HQz1**–**HQz6**) and (**Qz-OMe**).

## Absorption and emission spectrum

Absorption and emission spectra of **HQz1**–**HQz6** have been acquired in THF at room temperature. Their absorption spectra displayed bands at 240–258 nm with high molar extinction coefficients owing to π–π* transition in aromatic rings and another at 340–390 nm due to n–π* transition (Table 1 and Figure S20).[11b]

| | $\lambda_{ab}$/nm | $\lambda_{em}$/nm |
|---|---|---|
| **HQz1** | 254, 340 | 418 |
| **HQz2** | 257, 351 | 417 |
| **HQz3** | 244, 351 | 419 |
| **HQz4** | 258, 348 | 421 |
| **HQz5** | 256, 355 | 427 |
| **HQz6** | 240, 390 | 430 |

**Table 1**. Absorption and emission maxima for **HQz1**–**HQz6** ($\lambda_{ab}$=absorption maxima, $\lambda_{em}$=emission maxima)**.**

Upon excitation at longer wavelength absorption band, their emission spectra displayed a band with normal Stokes shift (<100 nm) associated with enol species of these derivatives in the range 415–430 nm (Table 1 and Figure S20).[11b]

The effect of polarity on the emission behaviour of these compounds (**HQz1**–**HQz6**) has been investigated in solvents with varying polarities. Their emission spectra displayed an analogous pattern in different solvents as observed in THF with normal emission band at 415–430 nm (Figures S21–S23). Thus it can be concluded that keto tautomers of these derivatives do not fluoresce in solvents of diverse polarities. It is presumed that keto form exists in solution in the form of dipolar species arising from electronic conjugation between donor and acceptor unit of the keto species.[2c,2d,14] In addition, dipolar species have freedom to adopt twisted conformations due to single bond rotations. Thus, emission of conformationally twisted dipolar species for **HQz1**–**HQz6** may be quenched through non-radiative decay process due to electronic push-pull effect and intramolecular rotations (discussed *vide-infra*; mechanism section).[2c,2d,14]

## Aggregation-Induced Emission

Emission behaviour of **HQz1**–**HQz6** in aggregated states has been followed in THF/water mixture with varying water volume fractions ($f_w$). Absorption spectra of these compounds showed insignificant changes with increasing $f_w$, up to 60%, but at 70% it broadened to a large extent. As well, it exhibited a red shift (~30 nm) and lowering of the absorption intensity.

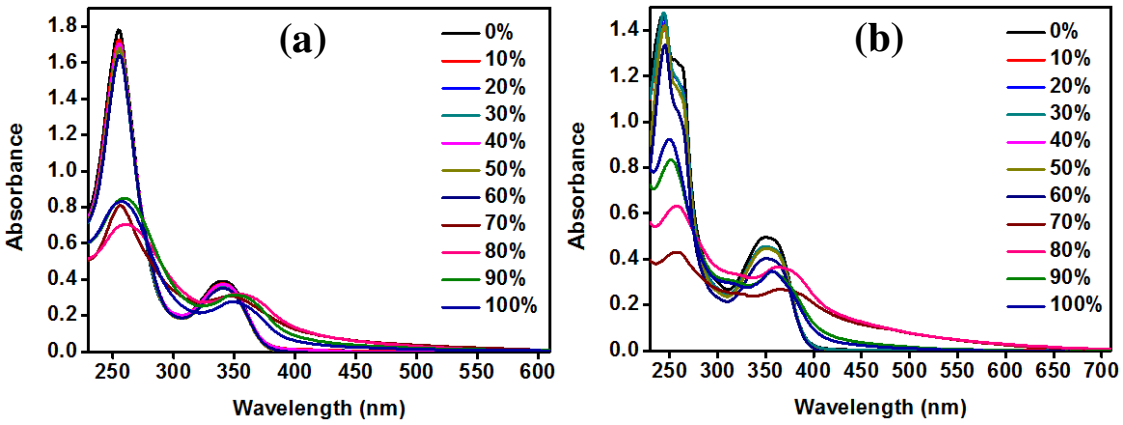


**Figure 1**. Absorption spectra of **HQz1** (a) and **HQz2** (b) in THF/water mixture with increasing $f_w$, (c, 50 μM, THF).

Further increase in $f_w$, up to 99% also showed broadening of the bands and lowering of intensity. Broadening of the spectral bands at higher $f_w$, known as 'levelling-off tail' is

usually observed in nanoaggregate suspensions due to Mie scattering.[15] It is consistent with typical AIE features and supported the formation of nanoaggregates (Figure 1, Figure S24 and Table S1). Red shifting of the absorption band with broadening indicated the possibility of J- aggregates.[16]

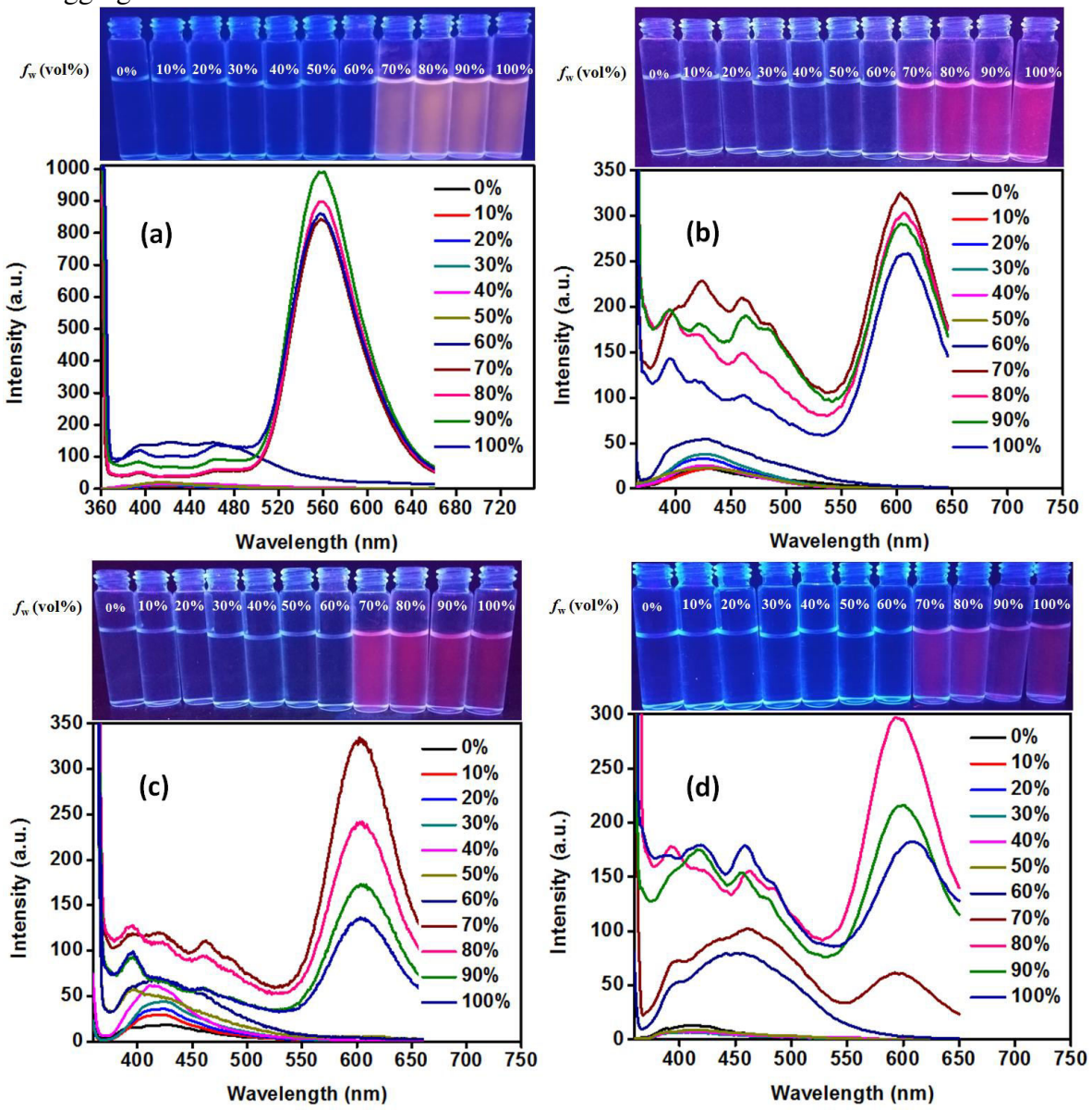


**Figure 2**. Emission spectra for **HQz1** (a), **HQz2** (b), **HQz3** (c) and **HQz4** (d) in THF/water mixtures with increasing $f_{w,}$ (c, 50 μM, THF).

To investigate the emission behaviour of **HQz1**–**HQz6** during aggregation, luminescence spectra have been acquired in the same solvent system (Figure 2, and Figure S25). Their emission spectra remained unchanged except showing small intensity enhancement due to enol emission at shorter wavelengths (400–450 nm) upon addition of water up to 60% to its THF solution. Further addition of water (beyond $f_w$ > 60%) led to the emergence of an intense band at a longer wavelength which intensified up to 99% $f_w$, with very large Stokes shift (up

to 314 nm) (Table S1). The emission band with a large Stokes shift at high water fraction may be attributed to emission due to excited keto form.[17] But in THF or at low $f_{w,}$ enol form dominated and got stabilized *via* hydrogen bonding with solvent molecules. Thus, large emission enhancement at high $f_{w,}$ represents the typical AIE feature and supported aggregation in **HQz1**–**HQz6**.[15] It is worth mentioning that the degree of aggregation and position of the emission bands (blue/red shifting) are distinct for each system.

The emission maxima for these compounds (**HQz1**–**HQz6**) lies in the range 560–701 nm [560, **HQz1**; 609, **HQz2**; 609, **HQz3**; 602, **HQz4**; 635, **HQz5**; 701, **HQz6**] with an apparent red shift due to increasing electron-donation ability of the substituents (**$R_1$**). However, the extent of aggregation showed reverse pattern, the intensity of the emission maxima went down from 84 times for **HQz1** to 3 for **HQz6** [84, **HQz1**; 35, **HQz2**; 58, **HQz3**; 23, **HQz4**; 8, **HQz5**; 3, **HQz6**] with increasing electron-donating ability of the substituent. Calculated fluorescence quantum yields in the aggregated state quantify the emission enhancement due to aggregation for **HQz1**–**HQz6** and gave fair idea of AIE and effect of substituent on AIE (Table S2).

**Solid-State Fluorescence**

As shown in Figure 3a, compounds **HQz1**–**HQz6** displayed broad and dual emission in the solid-state spread over 400–704 nm.[18] In their emission spectra, high energy bands (range 480–500 nm) due to typical enol form lies almost in the same region. On the other hand, lower energy band arising due to keto form displayed red shift with increasing electron donating nature of the substituent (**$R_1$**) (Table 2).[18]

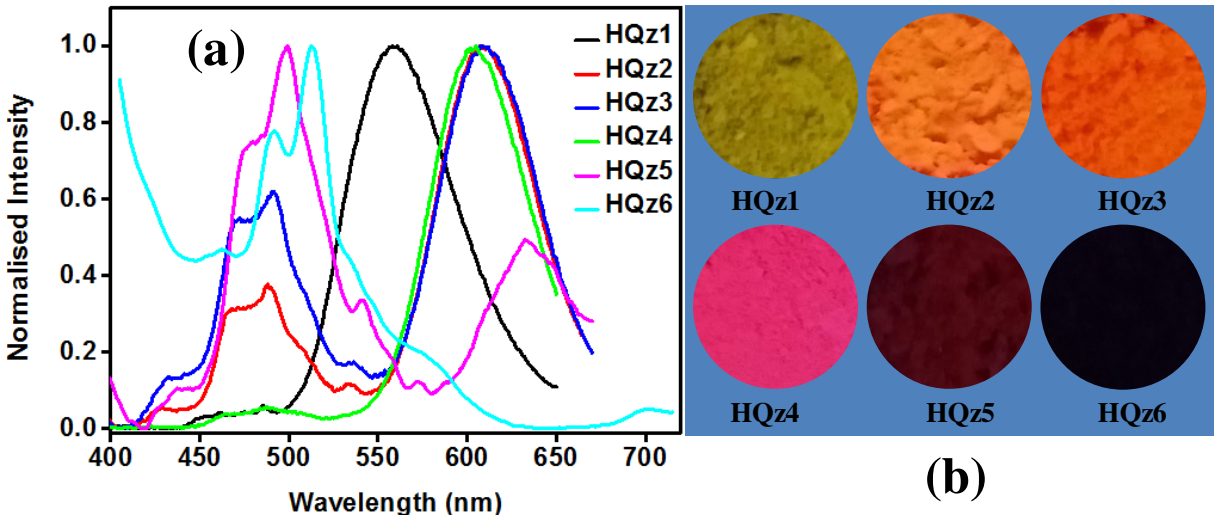


**Figure 3**. Normalised solid-state emission spectra (a) and photographs (b) of photo-luminescence for powder under UV irradiation ($\lambda_{ex}$, 365 nm) recorded for **HQz1**–**HQz6**.

The photograph of solid-state luminescence for **HQz1**–**HQz6** (powder) under UV light illumination ($\lambda_{ex}$, 365 nm) are depicted in Figure 3b. Emission wavelengths and their shifting pattern in the solid-state followed the same trends as in aggregated states for these derivatives. A comparison revealed that substituent (**$R_1$**) alters the proton transfer process and stability of the keto species in the excited state and causes an apparent change in the solid-state emission even in closely related systems.

| | $\lambda_{ex}$/nm | $\lambda_{em}$/nm (enol emissions) | $\lambda_{em}$/nm (Keto emissions) |
|---|---|---|---|
| **HQz1** | 340 | 465, 485, | 560 |
| **HQz2** | 351 | 473, 493 | 609 |
| **HQz3** | 351 | 472, 492 | 609 |
| **HQz4** | 348 | 470, 488 | 603 |
| **HQz5** | 355 | 475, 499 | 635 |
| **HQz6** | 390 | 491, 513 | 704 |

**Table 2.** Emission maxima of solid-state fluorescence for **HQz1–HQz6** ($\lambda_{ab}$=absorption maxima, $\lambda_{em}$=emission maxima)

**Computational Considerations**

Structural, photophysical properties and their correlation with **HQz1**–**HQz6** have further been explained by theoretical studies. In this regard, electronic structures of these derivatives and tautomeric forms have been optimized by DFT calculations using (B3LYP 6-31G**) method (Figure 4, and Figures S38–S42). Frontier molecular orbitals for **HQz1**–**HQz6** due to enol form are illustrated in Figure S41. The highest occupied molecular orbitals (HOMOs) for this form are spread over the entire system except for the formyl group, while their lowest unoccupied molecular orbitals (LUMOs) are mainly distributed on quinazoline moiety and formyl group. It is rational because the quinazoline moiety and formyl group may serve as proton acceptor for the ESIPT process. Moreover, it should be noted that hydroxy group and substituents (**$R_1$**) are fully entailed in HOMOs, and support the assumption that substituents (**$R_1$**) affect HOMOs to a greater extent than LUMOs. Further, frontier molecular orbitals for keto form have also been examined wherein HOMO is located on hydroxy-phenyl group and LUMO mainly on quinazoline moiety (Figure 4). Notably, with the introduction of strong electron donating groups (–**OMe**) in phenyl ring for **HQz6,** both HOMO and LUMO for this compound are populated only on the central hydroxy-phenyl ring. This indicated the prime role of the formyl group as an acceptor for **HQz6** (Figure 4, and Figure S42). Additional phenyl ring of the quinazoline moiety contributed mainly to LUMOs for both the tautomers. The energy of both HOMO and LUMO enhanced with increasing electron donor ability of

the substituent. As well, the energy of the HOMO enhances more steeply than LUMO which indicated that substituent ($\mathbf{R_1}$) makes a greater contribution to HOMO relative to the LUMO. It may be ascribed to localized electron density on the hydroxy-phenyl ring in HOMO relative to LUMO.

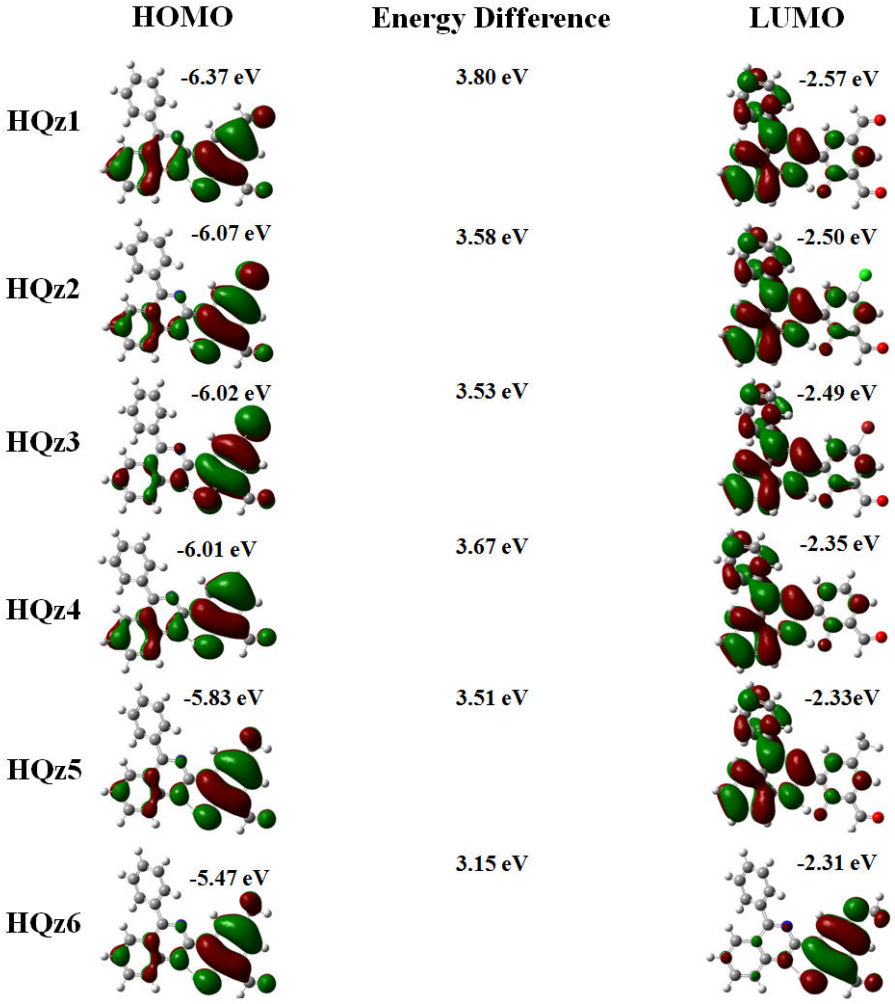


**Figure 4**. Frontier molecular orbitals (FMOs) of keto tautomers and their energies for **HQz1**–**HQz6**.

It has been concluded that inclusion of an electron donating group at hydroxy-phenyl ring causes an increase in the energy of HOMO, thus energy for lowest lying transition decreases. In contrary, the addition of an electron withdrawing substituent causes inverse effect, the energy for lowest lying transition increases due to lowering of energy for HOMO. UV/Vis spectral pattern from TD-DFT calculations are comparable with experimental results (Figures S43–S45). As evident from TD-DFT calculations on **HQz1**–**HQz6**, the lowest-energy absorption bands (electronic transition) observed in the UV/Vis spectra are mainly contributed by HOMO−LUMO transition alone (Figures S43–S45, and Table S10).

**Time-Resolved Fluorescence Spectra**

To gain deep insight into emission behaviour during aggregation, time-resolved spectra for **HQz1**–**HQz6** has been acquired in THF and different THF/water mixtures. The ensuing data in pure THF and different water fractions (10% to 99%) have been fitted with tri-exponential decays with three different components (Figure 5, Figure S29, and Tables S4–S9).

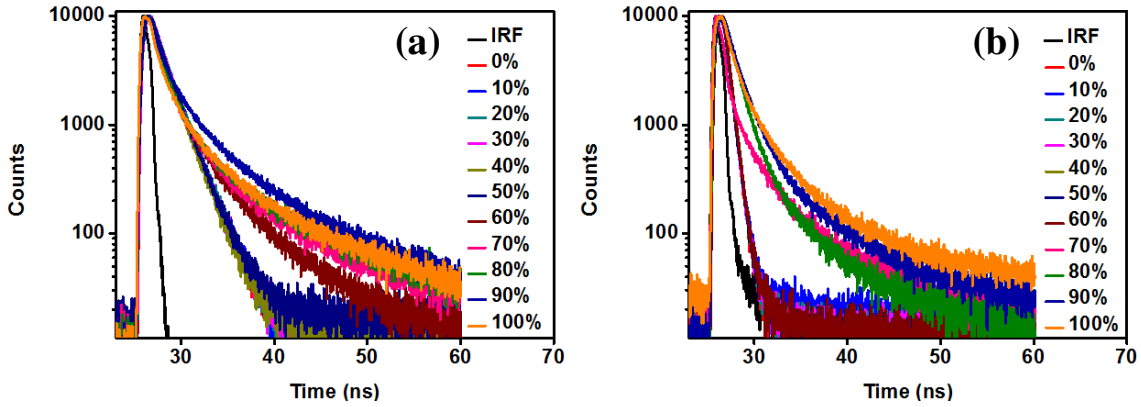


**Figure 5**. Time-resolved emission decay profiles for **HQz1** (a) and **HQz2** (b) at varying $f_w$, for (c, 50 μM, THF).

As an example, the main feature of **HQz1** for which data was acquired in THF and THF/water mixtures has been discussed. It showed fluorescence decay having three decay values 0.89 ns (τ1), 0.37 ns (τ2) and 0.39 ns (τ3) with respective abundances of 61%, 7.67%, and 31.33% respectively (Table S4). The observed fluorescence lifetime in THF is very small and may be attributed to emission due to the enol species. Further, data obtained with increasing water fraction up to 60% gave the profile analogous to that observed in THF with small fluorescence lifetime. On the other hand, it showed an enhanced lifetime at $f_w$, 70 to 99%. The enhanced fluorescence lifetime at higher water fraction may be attributed to an increase in fluorescence intensity in the aggregated state *via* an ESIPT process due to the keto species. Time-resolved fluorescence data for other derivatives (**HQz2**–**HQz6**) displayed the similar trend in terms of profile and lifetime (Tables S4–S9, and Figure S29). In fact, small fluorescence lifetime in THF and low water fraction may be attributed to enol species and enhanced fluorescence lifetime in higher water fraction to keto form. Moreover, various non-radiative channels through active intramolecular rotation and charge transfer processes may also be responsible for lower fluorescence lifetime. At higher water fraction various non-radiative decay processes are physically restrained due to aggregation, therefore fluorescence

lifetime is enhanced. Conclusively, enhanced fluorescence lifetime at higher water fraction supported the AIE and ESIPT process.[15,19]

**Aggregate Morphology**

To understand the intricacies of aggregation process and optical responses by varying the substituent, SEM images for **HQz1**–**HQz6** have been obtained in THF/water mixture (2:8) (Figure 6). The images revealed that the shape of nanoaggregate strongly depends on substituents ($\mathbf{R_1}$) which define the arrangement of the aggregates. Although, these compounds (**HQz1**–**HQz6)** displayed unique morphology, among these the shape of **HQz6** was entirely different. As shown in Figure 6, the aggregates for **HQz1**, **HQZ3** and **HQz4** consisted of nanorods, **HQz2** entangled thread like nanoparticles, while **HQz6** nanospheres. A closer look at SEM images for **HQz1**–**HQz5** showed the existence of more than one hierarchical assembly. Along with the aforesaid shape for each derivative (Figure 6) some spherical and block-shaped nanostructures too occur indicating the presence of more than one type of species in the aggregated state.[19]

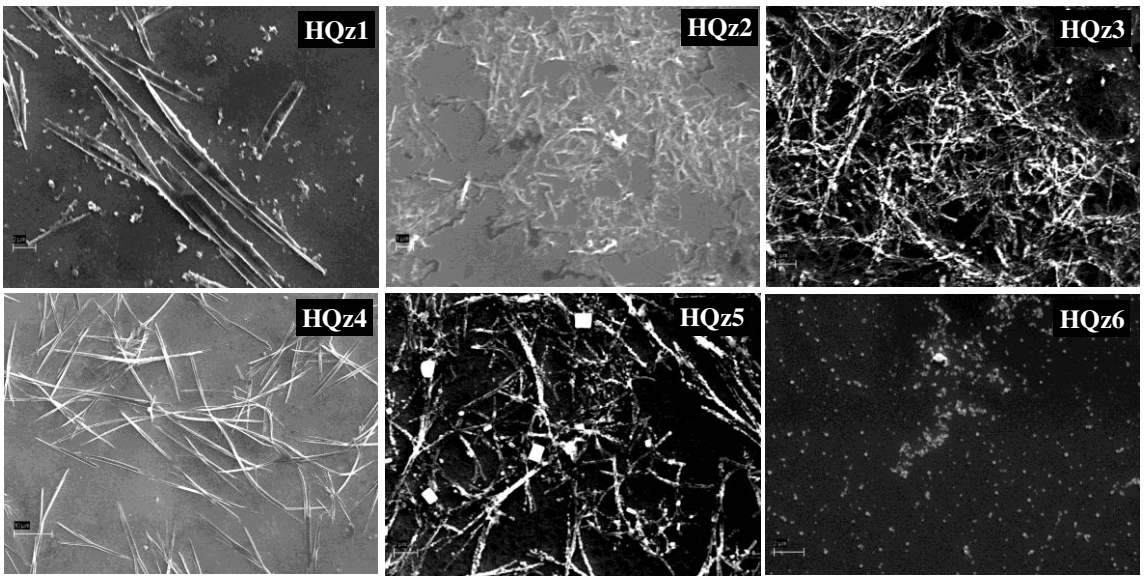


**Figure 6**. SEM images of the aggregates for **HQz1**–**HQz6** formed in a mixture of THF/water ($f_w$ 80 %; c, 50 μM in THF).

**Mechanistic Aspects**

To ensure the occurrence of ESIPT in these derivatives (**HQz1–HQz6**) a non-proton model compound (**Qz-OMe**) having methoxy in place of the hydroxy group has been synthesized and its emission spectra acquired in THF and THF/water mixture (Figures S26–S27). Emission spectra of **Qz-OMe** showed a band at a shorter wavelength (400–450

nm) in THF and THF/water mixture, and even at higher water fractions. Notably, it did not show any band at higher wavelengths (550 to 700 nm) which clearly indicated the nonexistence of ESIPT due to the lack of hydroxy-proton in **Qz-OMe**.[13] Thus, higher energy band has been unambiguously assigned to enol emission and the lower one to keto tautomers of **HQz1–HQz6**. This observation supported the involvement of proton transfer and keto species during aggregation and accordingly, the dominance of keto tautomer in the aggregated state. Thus, we can conclude that ESIPT emission can be restored through AIE with good quantum yields and to the best of our knowledge this is the first report where frustrated ESIPT emission is restored through AIE. Besides, it is worth noting that **Qz-OMe** also showed emission enhancements (AIE) with increasing water fraction in THF/water mixtures at a shorter wavelength (~450 nm) (Figures S27–28).

Moreover, it is noteworthy to mention that the inclusion of formyl group (*o*- to the hydroxy group) in these derivatives (**HQz1**–**HQz6**) is essential to activate the ESIPT process. In want of the formyl group on the central phenyl ring, these derivatives (**3a**–**3e)** do not show AIE and considerable solid-state fluorescence despite fulfilling ESIPT requirements (Figures S31–S37 and Table S3). This negative result for **3a**–**3e** may probably be due to weak hydrogen bonding and low acidity of the hydroxy protons, thus poor chances for ESIPT. To have an idea about the acidity of the hydroxy proton and consequently intramolecular hydrogen bonding in **3a**–**3e** and **HQz1**–**HQz6**, $^1$HNMR spectral studies have been performed (Table 3 and Figures S1–S11). Expectedly $^1$HNMR spectra of the respective compounds showed a small downfield shift ($\delta$) for hydroxy protons of **3a**–**3e** relative to those for **HQz1**–**HQz6** which clearly indicated poor hydrogen bonding and low acidity for the hydroxy proton (Table 3).[20]

| Compounds | $^1$H NMR Shift ($\delta$) | Compounds | $^1$H NMR Shift ($\delta$) |
|---|---|---|---|
| **3a** | 13.88 ppm | **HQz1** | 15.99 ppm |
| **3b** | 13.89 ppm | **HQz2** | 15.03 ppm |
| **3c** | 13.86 ppm | **HQz3** | 14.98 ppm |
| **3d** | 13.78 ppm | **HQz4** | 14.97 ppm |
| **3e** | 13.45 ppm | **HQz5** | 14.70 ppm |
| | | **HQz6** | 14.38 ppm |

**Table 3**. $^1$HNMR chemical shift ($\delta$) for hydroxy proton in **3a**–**3e** and **HQz1**–**HQz6**

It is well established that many fluorophores with rotating units are non-fluorescent in solution, however fluorescence revival occurs in aggregated/solid state due to physical restraints on intramolecular rotations.[15] To affirm the influence of RIR in AIE, viscosity

measurements have been performed in methanol/glycerol mixture with increasing glycerol fractions ($f_g$) (Figure 7 and Figure S30). In methanol, an emission band appeared at shorter wavelength [$\lambda_{em}$/nm, 450, **HQz1**; 423, **HQz2**; 423, **HQz3**; 423, **HQz4**; 424, **HQz5**; 460, **HQz6**] due to enol and upon gradual increase of the glycerol fraction, intensity of the band enhanced incessantly due to the restriction of active intramolecular rotations. Further, a distinct band emerged at higher wavelength [$\lambda_{em}$/nm, 560, **HQz1**; 606, **HQz2**; 606, **HQz3**; 602, **HQz4**] along with the one at shorter wavelength when glycerol fraction reached 70%. Further continual intensity enhancement occurred upon increasing the glycerol fraction up to $f_g$, 90%. The appearance of a lower energy band at high glycerol fraction supported the existence of keto species in the viscous medium. Thus, we conclude that keto species dominate in solid/aggregated states and viscosity measurements supported the influence of RIR and existence of keto species in the aggregated state too.[15]

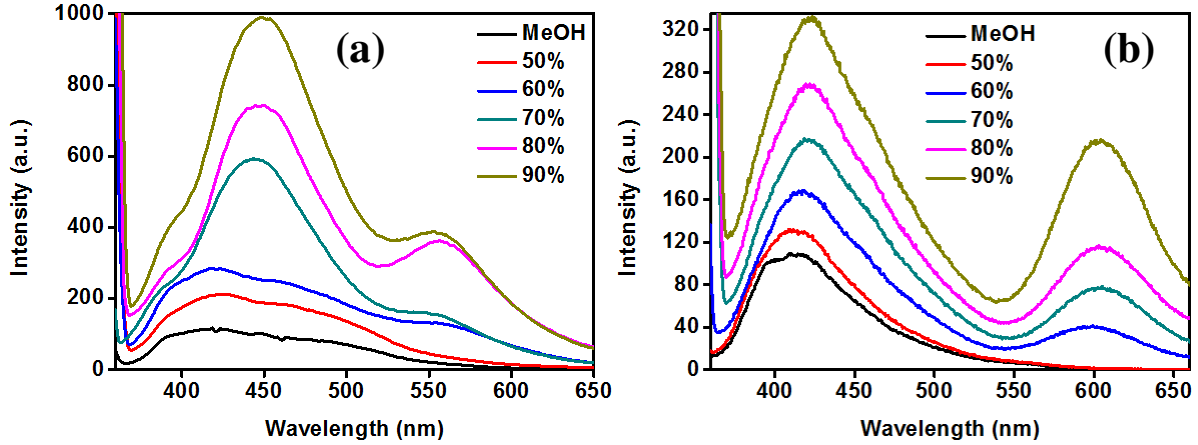


**Figure 7**. Emission spectra of **HQz1** (a), and **HQz2** (b) in methanol/glycerol mixtures with varying glycerol volume fractions (c, 50 μM, THF).

As in the aggregated state at higher water fraction, fluorescence improved due to the formation of keto species *via* proton transfer under irradiation for **HQz1**–**HQz6**. The compound **HQz1** showed yellow light (560 nm) and most intense emission relative to other derivatives whereas **HQz6** displayed the least intense emission and most red-shifted band (~701 nm). It is very interesting to observe that emission maxima for these derivatives exhibited dramatic red shift with increasing electron donating ability of the substituent and degree of aggregation lowered. To explain the substituent effect on emission profiles of **HQz1**–**HQz6** in the aggregated state, we consider possible keto species of these derivatives as illustrated in Figure 8. Two keto species (non-ionic) may be formed during proton transfer reactions **A2** and **A5**. Among these, **A2** is a planar and rigid system with greater accessibility

for conjugation and poor chances for active intramolecular rotation. Thus, it can be believed that form **A2** may be more stable and highly fluorescent relative to **A5** in solid/aggregated state. The keto form **A5** arising through the ESIPT process between the formyl group and the central hydroxy-phenyl ring is less planar and may be more accessible for intramolecular rotations due to lack of H–bonding between the central hydroxy-phenyl ring and the quinazoline moiety. In addition, the system can easily adopt a twisted structure through active intramolecular rotations. Consequently, keto form **A5** can be expected to display red-shifted bands relative to **A2**. Further, the substituent (**$R_1$**) with electron withdrawing nature makes the central phenyl ring electron deficient in addition to enhancing acidity of the hydroxy proton without affecting the basicity of the quinazoline nitrogen, thus it becomes easier to take advantage of a proton for hydrogen bonding and ESIPT process. At the same time, electron withdrawing nature of **$R_1$** stabilizes keto tautomer through proper electronic conjugation due to appropriate position.[2c] Thus, it can also be believed that keto form **A2** is the major species in aggregated/solid states of these derivatives with electron withdrawing substituent, therefore the system restores a large fluorescence with small red-shift arising from additional planarity.[13] Accordingly, **HQz1** with electron withdrawing substituent (–CHO) displays a large emission enhancement with small red-shift (at ~560 nm) relative to other derivatives.

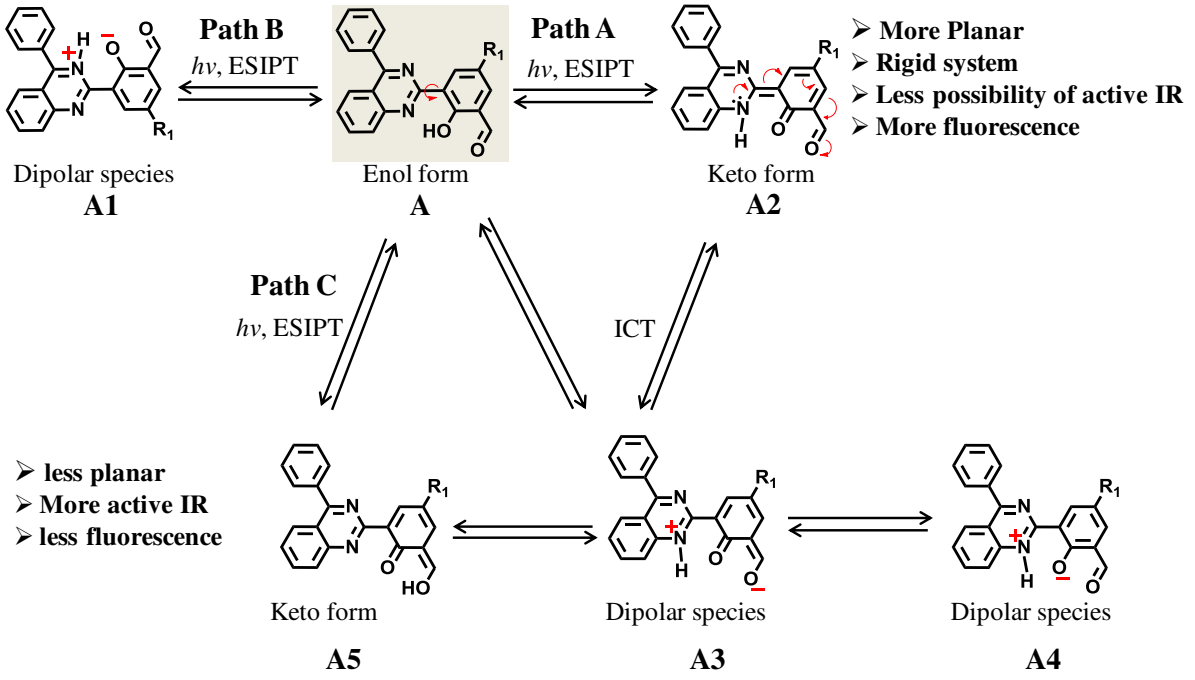


**Figure 8**. Representation of the general mechanistic scheme for **HQz1–HQz6** (IR=intramolecular rotation).

Interestingly, derivatives having –Cl (**HQz2**) and –Br (**HQz3**) also showed good AIE because of their –I (inductive) and ring deactivating effect, making the proton acidic required for the ESIPT process. **HQz4** (substituent, –H) also showed considerable AIE due to the moderate acidity of a hydroxy proton which is necessary for fast ESIPT process. On the other hand, the $-CH_3$ (**HQz5**) and $-OCH_3$ (**HQz6**) derivative showed poor AIE with large red shifted bands relative to other derivatives as $-OCH_3$/$-CH_3$ makes the ring electron rich due to strong electron releasing nature. At the same time, these bring down the acidity of the hydroxy proton and subsequently, the system becomes less susceptible for proton transfer (Table 3, and Figures S10–S11). Thus, for quinazoline derivatives with electron releasing group, keto form destabilizes and enol dominates. Substituent position in the central phenyl ring (*p*- to the hydroxy) also plays an important role in the destabilization of the keto species to a greater extent and equilibrium shifts to the enol side. It is also believed that keto form **A5** exists in the aggregated state of the $-OCH_3$ derivative, which is responsible for large red-shifting of the AIE band. Keto form **A5** may display lower fluorescence with additional red shifting because the molecules can adopt twisted conformation due to the intramolecular rotation.[14a] SEM images (aggregate morphology) also supported the assumption that **HQz6** involves different species in the aggregated state than other derivatives because it displayed an entirely different aggregate morphology (Figure 6; *vide-supra)*. DFT calculations further suggested the existence of keto form **A5** for **HQz6**, because HOMO and LUMO of the keto tautomer for this molecule are concentrated mainly on the central hydroxy-phenyl ring. However, for other derivatives, it involves both the moieties (central hydroxy-phenyl and quinazoline) (Figure 4 and Figure S42). Thus, the experimental results indicated that the formyl group serves as a proton acceptor for ESIPT in **HQz6**. As shown in Figure 8, the possibility of dipolar species (**A1**, **A3**, and **A4**) due to ICT in the keto species and ESIPT in the rotamers of **HQz1**–**HQz6** cannot be ruled out.[2c, 2d, 20b] Thus, it can be concluded that the keto form exists in solution (in various solvents) as a dipolar species due to strong push-pull interaction and, their emission is quenched due to non-radiative decay process.[2c, 2d, 20b] On the other hand, in aggregated/solid state, the intense band arises due to the non-ionic keto isomers (**A2/A5**) of these derivatives.

## Conclusion

Through this work, a novel family of ESIPT active quinazoline-based fluorophores has been developed wherein ESIPT emission is fully frustrated in polar and non-polar solvents. In

these fluorophores, ESIPT emission has been successfully restored through AIE with extremely large Stokes shift up to 314 nm. These exhibited solid-state fluorescence which has been tuned from 455 to 704 nm. The formyl group in these derivatives serves as a switch to activate ESIPT and, thereby causes AIE and solid-state fluorescence. Electron donating substituted derivatives causes longer wavelength emission in aggregated/solid state, while those with electron withdrawing a lower emission wavelength. The occurrence of the ESIPT and AIE has been directly correlated to the acidity of hydroxy proton of these derivatives. Thus, the study provides a first detailed account of AIE in the quinazoline derivatives *via* ESIPT with the largest Stokes shift observed so far for the same system. Also, this is the first report dealing with the systems where frustrated ESIPT emission is restored through AIE with good quantum yield.

## Experimental Section

### Reagents

The solvents were dried and distilled prior to use following standard literature procedures.[21] 2-Aminobenzophenone, salicylaldehyde, 5-chlorosalicylaldehyde, 5-bromo-salicylaldehyde, 5-methylsalicylaldehyde, 5-methoxysalicylaldehyde, hexamine ($C_6H_{12}N_4$), iodine ($I_2$), iodomethane and trifluoroacetic acid were procured from Sigma Aldrich, India and used as received without further purifications.

### General Information

$^1H$ and $^{13}C$ spectra have been acquired on a JEOL AL 500 FT-NMR spectrometer using tetramethylsilane (TMS) as an internal reference. High-resolution mass spectra (HRMS) have been recorded on a Bruker Daltonics Amazon SL ion trap mass spectrometer (micrOTOF-Q II 10348) by the electrospray ionization (ESI) method. Electronic absorption and fluorescence spectra have been acquired on Shimadzu UV-1800 and Perkin-Elmer *LS* 55 spectrometers, respectively. SEM images were obtained on a JEOL JSM 840A scanning electron microscope. Time-resolved fluorescence (TRF) decay measurements were carried out using a time-correlated single photon counting (TCSPC) system from Horiba Yovin (Model: Delta Flex). Samples were excited using a picoseconds diode laser (Model: Delta Diode) and data analysis performed using EzTime (HORIBA Scientific) decay analysis software. Fluorescence quantum yield ($\Phi_F$) for these samples has been calculated relative to rhodamine 6G dye ($H_2O$, $\lambda_{ex}$=530 nm, $\lambda_{em}$=552 nm, $\Phi$=0.95) as a reference using the following formula $[(\Phi_F=\Phi_R \times (I_T/I_R) \times (A_R/A_T) \times (\eta_T^2/\eta_R^2)]$, where $\Phi$=quantum yield, I=area under the curve of

emission spectrum, A=absorbance at $\lambda_{ex}$, η=refractive index of solvent. The subscript R and T denote the values for the reference substance and test samples respectively.

**Synthesis of 4-hydroxy-5-(4-phenylquinazolin-2-yl)isophthalaldehyde (HQz1)**

A mixture of 3a (596.68 mg, 2 mmol) and hexamethylenetetramine (1121.49 mg, 8 mmol, 4 eq) was refluxed in trifluoroacetic acid (10 ml) for 9 hours at 100˚C. To ensure complete consumption of 3a progress of the reaction was monitored by TLC. Subsequently, the reaction mixture was cooled to room temperature and a solution of 4M HCl (30 ml) was added to it and allowed to stir for an additional 01 hour to afford a yellow precipitate. The resulting precipitate was filtered, washed with water and dried in vacuum to afford the desired product. It was purified by the silica gel column chromatography using dichloromethane/*n*-hexane (1:4) as eluent to yield yellow solid (**HQz1**). Yield: 680 mg (96%). **$^1$H NMR** (500 MHz, $CDCl_3$) *δ*=15.99 (s, 1H), 10.67 (s, 1H), 10.03 (s, 1H), 9.51(d, *J*=1.5 Hz, 1H), 8.48 (d, *J*=2 Hz, 1H), 8.23 (d, *J*=8.5 Hz, 1H), 8.14 (s, 1H), 8.03 (s, 1H), 7.90 (t, *J*=5.5 Hz, *J*=2 Hz, 2H), 7.68 ppm (m, 4H); **$^{13}$C NMR** (125 MHz, $CDCl_3$) *δ*=190.32, 189.02, 168.44, 136.64, 136.28, 135.34, 134.16, 131.04, 130.27, 129.04, 128.56, 127.88, 125.13, 121.85, 121.28 ppm; **IR** (KBr pellet): 3421, 2956, 2925, 2854, 1691, 1602, 1535, 1467, 1388, 1218, 1137, 1096, 999, 770, 694, 537 $cm^{-1}$; **HRMS** (ESI): m/z calcd for $C_{22}H_{14}N_2O_3$ $[M+H]^+$: 355.1083; found: 355.1077.

**Synthesis of 5-chloro-2-hydroxy-3-(4-phenylquinazolin-2-yl)benzaldehyde (HQz2)**

It was synthesized following the above procedure for **HQz1** using **3b** (665.56 mg, 2 mmol) in place of **3a**. It was isolated as a yellow solid. Yield: 692 mg (92%). **$^1$H NMR** (500 MHz, $CDCl_3$) *δ*=15.03 (s, 1H), 10.60 (s, 1H), 9.07 (d, *J*=2 Hz, 1H), 8.20 (d, *J*=8.5 Hz, 1H), 8.12 (d, *J*=9.5, 1H), 8.06 (s, 1H), 8.01 (d, *J*=7 Hz, 1H), 7.87 (s, 2H), 7.67 ppm (m, 4H); **$^{13}$C NMR** (125 MHz, $CDCl_3$) *δ*=189.29, 162.64, 158.84, 136.39, 135.85, 135.65, 131.68, 131.10, 130.64, 129.10, 128.75, 127.10, 125.86, 124.75, 122.38 ppm; **IR** (KBr pellet): 3434, 3075, 2957, 2927, 2854, 1740, 1682, 1596, 1454, 1386, 1255, 1210, 1126, 1013, 936, 889, 777, 892, 633, 596 $cm^{-1}$; **HRMS** (ESI): m/z calcd for $C_{21}H_{13}ClN_2O_2$ $[M+H]^+$: 361.0744; found: 361.0738.

**Synthesis of 5-bromo-2-hydroxy-3-(4-phenylquinazolin-2-yl)benzaldehyde (HQz3)**

This compound was synthesized following the above procedure for **HQz1** using **3c** (754.46 mg, 2 mmol) in place of **3a**. It was separated as a yellow solid. Yield: 763 mg (94%).

**$^1$H NMR** (500 MHz, $CDCl_3$) $\delta$=14.98 (s, 1H), 10.59 (s, 1H), 9.07 (d, *J*=3 Hz, 1H), 8.19 (s, 1H), 8.05 (d, *J*=3 Hz, 1H), 8.00 (s, 1H), 7.88 (t, *J*=5 Hz, *J*=2.5 Hz, 2H), 7.66 ppm (m, 4H); **$^{13}$C NMR** (125 MHz, $CDCl_3$) $\delta$=188.64, 162.91, 138.27, 135.25, 134.37, 130.99, 130.25, 129.01, 128.45, 127.78, 127.62, 122.55, 121.71, 111.51 ppm; **IR** (KBr pellet): 3433, 3064, 2958, 2924, 1680, 1614, 1539, 1466, 1388, 1248, 1105, 974, 867, 777, 692, 671, 633, 608 $cm^{-1}$; **MS** (ESI): m/z calcd for $C_{21}H_{13}BrN_2O_2$ [M+K]+: 442.9; found: 443.0

**Synthesis of 2-hydroxy-3-(4-phenylquinazolin-2-yl)benzaldehyde (HQz4)**

It was prepared following the above procedure for **HQz1** with slight modifications. A mixture of **3a** (596.68 mg, 2 mmol) and hexamethylenetetramine (280.37 mg, 2 mmol, 1 eq) were refluxed at 70˚C in trifluoroacetic acid (10 mL) in a 100 ml round bottom flask with stirring for 6 hours and progress of the reaction monitored by TLC. After complete consumption of **3a,** reaction mixture was cooled and treated with 4M HCl (30 ml) and allowed to stir for an additional 01 hour until a yellow precipitate separated quantitatively. The precipitate was filtered, washed with water and dried under vacuum to afford yellow solid. The pure product was obtained by silica gel column chromatography using dichloromethane/*n*-hexane (1:9) as eluent. The first yellowish fraction was collected to afford yellow solid (**HQz4**). Yield: 254 mg (39%). **$^1$H NMR** (500 MHz, $CDCl_3$) $\delta$=14.97 (s, 1H), 10.67 (s, 1H), 9.00 (d, *J*=7.5 Hz, 1H), 8.18 (d, *J*=7.5 Hz, 1H), 8.10 (d, *J*=8.5 Hz, 1H), 7.97 (t, *J*=8.5 Hz, 2H), 7.88 (d, *J*=4 Hz, 2H), 7.64 (d, *J*=4 Hz, 4H), 7.07 ppm (d, *J*=7.5 Hz, 1H); **$^{13}$C NMR** (125 MHz, $CDCl_3$) $\delta$=189.91, 164.10, 136.29, 134.83, 132.12, 130.67, 130.13, 128.81, 127.86, 127.57, 124.76, 121.46, 120.63, 118.73 ppm; **IR** (KBr pellet): 3432, 3059, 2958, 2925, 2880, 2854, 1684, 1599, 1538, 1486, 1389, 1346, 1288, 1258, 1105, 915, 774, 753, 695, 673 $cm^{-1}$; **HRMS** (ESI): m/z calcd for $C_{21}H_{14}N_2O_2$ $[M+H]^+$: 327.1134; found: 327.1128.

**Synthesis of 2-hydroxy-5-methyl-3-(4-phenylquinazolin-2-yl)benzaldehyde (HQz5)**

This compound was synthesized following the above procedure for **HQz1** using **3d** (624.72 mg, 2 mmol) in place of **6a.** It was separated as yellow solid. Yield: 640 mg (94%). **$^1$H NMR** (500 MHz, $CDCl_3$) $\delta$=14.69 (s, 1H), 10.62 (s, 1H), 8.77 (d, *J*=2 Hz, 1H), 8.15 (d, *J*=8.5 Hz, 1H), 8.06 (s, 1H), 7.94 (s, 1H), 7.86 (t, *J*=4 Hz, *J*=3.5 Hz, 2H), 7.76 (d, *J*=2 Hz, 1H), 7.63 (m, 4H), 2.38 ppm (s, 3H); $^{13}$C NMR (125 MHz, $CDCl_3$) $\delta$=190.09, 162.25, 136.73, 134.87, 132.38, 130.73, 130.21, 128.91, 128.03, 127.87, 127.63, 124.53, 121.49, 120.40, 20.55 ppm; **IR** (KBr pellet): 3437, 3064, 2923, 2879, 1680, 1614, 1570, 1538, 1466, 1388, 1349, 1289, 1248, 1105, 974, 867, 777, 692, 671, 633, 608 $cm^{-1}$; **HRMS** (ESI): m/z calcd for

$C_{22}H_{16}N_2O_2$ [M+H]+: 341.1290; found: 341.1285.

**Synthesis of 2-hydroxy-5-methoxy-3-(4-phenylquinazolin-2-yl)benzaldehyde (HQz6)**

It was synthesized following the above procedure for **HQz4** using **3e** (656.72 mg, 2 mmol) in place of **6a**. It separated as yellow solid. Yield: 528 mg (74%). **$^1$H NMR** (500 MHz, $CDCl_3$) $\delta$=14.39 (s, 1H), 10.65 (s, 1H), 8.61 (d, *J*=4 Hz, 1H), 8.18 (d, *J*=8.5 Hz, 1H), 8.08 (s, 1H), 7.96 (s, 1H), 7.87 (t, *J*=5.5 Hz, *J*=2 Hz, 2H), 7.64 (t, *J*=5 Hz, *J*=5.5 Hz, 3H), 7.51 (d, *J*=4 Hz, 1H), 3.92 ppm (s, 4H); **$^{13}$C NMR** (125 MHz, $CDCl_3$) $\delta$=189.66, 158.91, 151.96, 134.88, 130.76, 130.26, 128.88, 128.01, 127.82, 127.63, 123.45, 121.57, 114.93, 56.17 ppm; **IR** (KBr pellet): 3438, 3077, 2926, 2855, 1680, 1572, 1539, 1463, 1394, 1348, 1304, 1245, 1216, 1098, 1049, 781, 768, 698, 633, 587 $cm^{-1}$; **HRMS** (ESI): m/z calcd for $C_{22}H_{16}N_2O_3$ [M+H]+: 357.1239; found: 357.1234.

**Synthesis of 5-bromo-2-methoxy-3-(4-phenylquinazolin-2-yl)benzaldehyde (Qz-OMe)**

A 100 ml round bottom flask containing DMF (20 ml) was charged with **HQz3** (810.48 mg, 2 mmol), $K_2CO_3$ (1105.64 mg, 8 mmol) and the reaction mixture stirred for an hour at RT. Afterwards, it was treated with iodomethane (250 µl, 4 mmol) and stirred for 24 hours at RT. After completion of the reaction, the mixture was poured into ice water and filtered to afford a white solid. The crude product was purified by silica gel column chromatography (hexane/$CH_2Cl_2$, 9:1 v/v) to obtain Qz-OMe as a white solid. Yield: 644 mg (77%). **$^1$H NMR** (500 MHz, $CDCl_3$) $\delta$=10.47 (s, 1H), 8.42 (d, *J*=3 Hz, 1H), 8.20 (d, *J*=8.5 Hz, 2H), 8.08 (d, *J*=2 Hz, 1H), 7.98 (s, 1H), 7.85 (d, *J*=4 Hz, 2H), 7.67 (s, 1H) 7.61 (t, *J*=2.5 Hz, *J*=3 Hz, 3H) 3.91 ppm (s, 3H); **$^{13}$C NMR** (125 MHz, $CDCl_3$) $\delta$=188.75, 168.94, 161.27, 158.73, 151.63, 140.96, 136.97, 135.66, 134.17, 132.31, 131.43, 130.25, 130.05, 129.16, 128.74, 128.20, 127.15, 121.48, 117.41, 64.63 ppm; **IR** (KBr pellet): 3060, 2940, 1981, 1805, 1688, 1564, 1538, 1487, 1456, 1386, 1213, 1161, 996, 925, 889, 877, 813, 776, 787, 692, 669, 656 $cm^{-1}$; **HRMS** (ESI): m/z calcd for $C_{22}H_{15}BrN_2O_2$ [M+H]+: 419.0395; found: 419.0390.

**Theoretical Studies**

Geometry optimization of **HQz1–HQz6** has been performed in singlet state using Density Functional Theory (DFT) with B3LYP hybrid functional and 6-31G** basis set.[22] The electronic spectra of these compounds have been calculated using Time-dependent DFT (TDDFT). All theoretical calculations were done using the Gaussian 09 program.[23]

**Acknowledgment**

We acknowledge financial support from the Science and Engineering Research Board (SERB), New Delhi, through the scheme **EMR/2015/001535**. B.K.D. acknowledges the University Grants Commission, New Delhi, India, for a Senior Research Fellowship (22/6/2014(i)EU-V).

**Keywords**: Quinazoline, Aggregation, Keto-enol tautomerisation, Fluoroscence, solid-state emissions

[1] a) S. Cherumukkil, S. Ghosh, V. K. Praveen, A. Ajayaghosh, *Chem. Sci.* **2017**, *8*, 5644–5649; b) P. Anees, J. Joseph, S. Sreejith, N. V. Menon, Y. Kang, S. W.-K. Yu, A. Ajayaghosh, Y. Zhao, *Chem. Sci*. **2016**, *7*, 4110–4116; c) L. Yuan, W. Lin, K. Zheng, L. He, W. Huang, *Chem. Soc. Rev*. **2013**, *42*, 622−661; d) Z. Guo, S. Park, J. Yoon, I. Shin, *Chem. Soc. Rev*. **2014**, *43*, 16–29.

[2] a) V. S. Padalkar, S. Seki, *Chem. Soc. Rev.* **2016**, *45*, 169−202; b) J. E. Kwon, S. Y. Park, *Adv. Mater.* **2011**, *23*, 3615–3642; c) D. Dahal, L. McDonald, X. Bi, C. Abeywickrama, F. Gombedza, M. Konopka, S. Paruchuri, Y. Pang, *Chem. Commun.* **2017**, *53*, 3697−3700; d) W. Chen, B. D. Wright, Y. Pang, *Chem. Commun.,* **2012**, *48*, 3824–3826; e) K. Skonieczny, J. Yoo, J. M. Larsen, E. M. Espinoza, M. Barbasiewicz, V. I. Vullev, C.-H. Lee, D. T. Gryko, *Chem. Eur. J*. **2016**, *22*, 7485 – 7496.

[3] a) M. Raoui, J. Massue, C. Azarias, D. Jacquemin, G. Ulrich, *Chem. Commun.* **2016**, *52*, 9216–9219; b) M.-W. Chung, T.-Y. Lin, C.-C. Hsieh, K.-C. Tang, H. Fu, P.-T. Chou, S.-H. Yang, Y. Chi, *J. Phys. Chem. A* **2010**, *114*, 7886–7891; c) D. T. Gryko, J. Piechowska, M. Galezowski, *J. Org. Chem.* **2010**, *75*, 1297−1300; d) P. Yang, J. Zhao, W. Wu, X. Yu, Y. Liu, *J. Org. Chem.* **2012**, *77*, 6166–6178; e) I. Deperasinska, D. T. Gryko, E. Karpiuk, B. Kozankiewicz, A. Makarewicz, J. Piechowska, *J. Phys. Chem. A* **2012**, 116, 12049−12055; f) E. Heyer, K. Benelhadj, S. Budzak, D. Jacquemin, J. Massue, G. Ulrich, *Chem. Eur. J.* **2017**, *23*, 7324−7336.

[4] a) J. Mei, Y. Hong, J. W. Y. Lam, A. Qin, Y. Tang, B. Z. Tang, *Adv. Mater.* **2014**, *26*, 5429–5479; b) J. Mei, N. L. C. Leung, R. T. K. Kwok, J. W. Y. Lam, B. Z. Tang, *Chem. Rev.* **2015**, *115*, 11718−11940; c) S. Li, J. Sun, M. Qile, F. Cao, Y. Zhang, Q. Song, *ChemPhysChem* **2017**, *18*, 1481 – 1485.

[5] a) X. Ma, R. Sun, J. Cheng, J. Liu, F. Gou, H. Xiang, X. Zhou, *J. Chem. Educ*. **2016**, *93*, 345–350; b) L. Peng, S. Xu, X. Zheng, X. Cheng, R. Zhang, J. Liu, B. Liu, A. Tong, *Anal. Chem.* **2017**, *89*, 3162−3168; c) J. B. Briks. Photophysics of Aromatic Molecules; wiley: New York **1970**.

[6] a) Y. Xu, Q. Liu, B. Dou, B. Wright, J. Wang, Y. Pang, *Adv. Healthcare Mater.* **2012**, *1*, 485–492; b) A. Matsui, K. Umezawa, Y. Shindo, T. Fujii, D. Citterio, K. Oka, K. Suzuki, *Chem. Commun*. **2011**, *47*, 10407; c) J. M. Baumes, J. J. Gassensmith, J. Giblin, J.-J. Lee, A. G. White, W. J. Culligan, W. M. Leevy, M. Kuno, B. D. Smith, *Nat. Chem.* **2010**, *2*, 1025.

[7] a) C. Huang, Y. Fu, H. Fu, Y. Jiang, Y. Zhao, *Chem. Commun.* **2008**, *47*, 6333–6335; b) F.-R. Chang, Y.-H. Lee, Y.-L. Yang, P.-W. Hsieh, A. T. Khalil, C.-Y. Chen, Y.-C. Wu, *J. Nat. Prod.* **2003**, *66*, 1245−1248; c) J. P. Michael, *Nat. Prod. Rep.* **2008**, *25*, 166–187.

[8] a) S. Srivastava, S. Srivastava, *Int. J. Pharm. Sci. Res.* **2015**, *6*, 1206−1213; b) R. Rajput, A. P. Mishra, *Int. J. Pharm. Pharm. Sci.* **2012**, *4*, 66 – 70; c) P. A. Ple, T. P. Green, L. F. Hennequin, J. Curwen, M. Fennell, J. Allen, C. L. D. Brempt, G. Costello, *J. Med. Chem*. **2004**, *47*, 871.

[9] a) M. K. Bera, C. Chakraborty, P. K. Singh, C. Sahu, K. Sen, S. Maji, A. K. Das, Sudip Malik, *J. Mater. Chem. B* **2014**, *2*, 4733–4739; b) H. Yin, H. Li, G. Xia, C. Ruan, Y. Shi, H. Wang, M. Jin, D. Ding, *Sci. Rep.* **2016**, *6*, 19774; c) S. Tsuchiya, K.-i. Sakai, K. Kawano, Y. Nakane, T. Kikuchi, T. Akutagawa, *Chem. Eur. J.* **2018**, *24*, 5868 – 5875.

[10] a) L. Yuan, W. Lin, S. Zhao, W. Gao, B. Chen, L. He, S. Zhu, *J. Am. Chem. Soc.* **2012**, *134*, 13510−13523; b) Y. Dai, H. Xiao, J. Liu, Q. Yuan, P. Ma, D. Yang, C. Li, Z. Cheng, Z. Hou, P. Yang, J. Lin, *J. Am. Chem. Soc*. **2013**, *135*, 18920–18929.

[11] S. K. Panja, N. Dwivedi, S. Saha, *Tetrahedron Letters* **2012**, *53*, 6167–6172; b) S. K. Panja, S. Saha, *RSC Adv*. **2013**, *3*, 14495−14500.

[12] C. Herrero, J. L. Hughes, A. Quaranta, N. Cox, A. W. Rutherford, W. Leibl, A. Aukauloo, *Chem. Commun.* **2010**, *46*, 7605–7607.

[13] S. Park, O.-H. Kwon, S. Kim, S. Park, M.-G. Choi, M. Cha, S. Y. Park, D.-J. Jang, *J. Am. Chem. Soc*. **2005**, *127*, 10070–10074.

[14] a) T. Mutai, H. Sawatani, T. Shida, H. Shono, K. Araki, *J. Org. Chem.* **2013**, *78*, 2482−2489; b) S. Kim, J. Seo, S. Y. Park, *J. Photochem. Photobiol. A: Chem.* **2007**

*191* 19–24; c) F. Vollmer, W. Retig, *J. Photochem. Photobiol. A: Chem.* **1996**, *95*, 143−155; d) M. I. Knyazhansky, A.V. Metelitsa, A. J. Bushkov, S.M. Aldoshin, *J. Photochem. Photobiol. A: Chem.* **1996**, *97,* 121−126; e) Y. Qian, M.-M. Cai, L.-H. Xie, G.-Q. Yang, S.-K. Wu, W. Huang, *ChemPhysChem* **2011**, *12*, 397 – 404.

[15] Y. Hong, J. W. Y. Lam, B. Z. Tang, *Chem. Commun*. **2009**, 4332–4353.

[16] A. Maity, F. Ali, H. Agarwalla, B. Anothumakkool, A. Das, *Chem. Commun.* **2015**, *51*, 2130–2133.

[17] a) Z. Song, R. T. K. Kwok, E. Zhao, Z. He, Y. Hong, J. W. Y. Lam, B. Liu, B. Z. Tang, *ACS Appl. Mater. Interfaces* **2014**, *6*, 17245−17254; b) Y. Qian, S. Li, G. Zhang, Q. Wang, S. Wang, H. Xu, C. Li, Y. Li, G. Yang, *J. Phys. Chem. B* **2007**, 111, 5861−5868.

[18] a) V. S. Padalkar, Y. Tsutsui, T. Sakurai, D. Sakamaki, N. Tohnai, K. Kato, M. Takata, T. Akutagawa, K.-i. Sakai, S. Seki, *J. Phys. Chem. B* **2017**, *121*, 10407−10416; b) K.-C. Tang, M.-J. Chang, T.-Y. Lin, H.-A. Pan, T.-C. Fang, K.-Y. Chen, W.-Y. Hung, Y.-H. Hsu, P.-T. Chou, *J. Am. Chem. Soc.* **2011**, *133*, 17738–17745; c) D. Yao, S. Zhao, J. Guo, Z. Zhang, H. Zhang, Y. Liu, Y. Wang, *J. Mater. Chem.* **2011**, *21*, 3568–3570.

[19] R. S. Singh, S. Mukhopadhyay, A. Biswas, D. S. Pandey, *Chem. Eur. J.* **2016**, *22*, 753−763.

[20] a) W.-T. Chuang, C.-C. Hsieh, C.-H. Lai, C.-H. Lai, C.-W. Shih, K.-Y. Chen, W.-Y. Hung, Y.-H. Hsu, P.-T. Chou, *J. Org. Chem.* **2011**, *76*, 8189−8202; b) W. Chen, E. B. Twum, L. Li, B. D. Wright, P. L. Rinaldi, Y. Pang, *J. Org. Chem*. **2012**, *77*, 285–290; c) Y.-A. Chen, F.-Y. Meng, Y.-H. Hsu, C.-H. Hung, C.-L. Chen, K.-Y. Chung, W.-F. Tang, W.-Y. Hung, P.-T. Chou, *Chem. Eur. J.* **2016**, *22*, 14688 –14695.

[21] D. D. Perrin, W. L. F. Armango, D. R. Perrin, Purification of laboratory Chemicals, Pergamon: Oxford, U.K. **1986**.

[22] a) W. R. Wadt, P. Hay, *J. Chem. Phys.* **1985**, *82*, 284–298; b) A. D. J. Becke, *Chem. Phys.* **1993**, *98*, 5648–5652.

[23] M. J. Frisch, G. W. Trucks, H. B. Schlegel, GAUSSIAN 09 Revision C. 01 Gaussian Inc. Wallingford CT. **2010**.

# Substituent Directed ESIPT Coupled AIE in NIR Emitting Quinazoline Derivatives

Mr. Bhupendra Kumar Dwivedi, Mr. Vishwa Deepak Singh, Dr. Rajendra Prasad Paitandi, and Prof. Dr. Daya Shankar Pandey*

Department of Chemistry, Institute of Science, Banaras Hindu University, Varanasi –221 005, (U. P.) India

**Abstract**

A series of ESIPT active systems (**HQz1**–**HQz6**) derived from quinazoline have been reported. The ESIPT emission for these derivatives gets completely quenched in solvents with diverse polarities which have been restored *via* AIE with large Stokes shift (up to 314 nm). It varied from 450 to 701 nm just by altering substituents at the para position of hydroxy group in the central phenyl ring. As well, **HQz1**–**HQz6** displayed solid-state emission [~ 455 (blue) to ~704 nm (red)]. The present study offers a simple route to obtain colour tunable ESIPT emission *via* AIE which is very important for biological imaging and fabrication of optoelectronic devices.